

Effect of Ductility Level on the Seismic Behavior of Low Reinforced Concrete Moment-Resisting Frames Equipped by Double Friction Pendulum Bearings Isolation

Seyed Ali Razavian Amraei ^{*1}; Seyed Amirhossein Ahmadi ²; Ayoub Shakouri ³; Gholamreza Ghodrati Amiri ⁴; Elham Rajabi ⁵

1. Associate Professor, Department of Civil Engineering, Payame Noor University, Tehran, Iran

2. M.Sc., Department of Civil Engineering, Payame Noor University, Tehran, Iran

3. Ph.D., Natural Disasters Prevention Research Center, School of Civil Engineering, Iran University of Science & Technology, Tehran, Iran

4. Professor, Natural Disasters Prevention Research Center, School of Civil Engineering, Iran University of Science & Technology, Tehran, Iran

5. Assistant professor, Qualitative and Quantitative Analysis of Fluids and Environmental Research Group, Department of Civil Engineering, Tafresh University, 39518-79611 Tafresh, Iran

* Corresponding author: razavian@pnu.ac.ir

ARTICLE INFO

Article history:

Received: 31 May 2024

Revised: 20 January 2025

Accepted: 09 March 2025

Keywords:

Base isolation;

Double friction pendulum bearing;

Level of ductility;

Nonlinear time history analysis;

Seismic effects.

ABSTRACT

The base isolation method is being utilized for more than two decades as a way to protect structures. Despite recent advancements in the seismic evaluation of isolated structures, the impact of ductility level on based-isolated Reinforced Concrete (RC) moment-resisting frame structures has not been explored. In order to consider the effect of ductility level, the present paper evaluates the seismic behavior of isolated RC moment-resisting frames through Double Friction Pendulum Bearings (DFPB) with ordinary, intermediate, and special ductility. Additionally, we compared responses of these systems with the similar conventional structures. To this end, three RC moment-resisting frame structures were designed with/without DFPB, and three-dimensional (3D) models were implemented in Open Sees. Then, seismic responses of these six models, including peak floor absolute acceleration, base shear, plastic rotation, and story drift of column were evaluated. According to the results. Ductility levels have a significant impact on the fixed and isolated structures. As a result of the special moment-resisting frame superstructure, plastic rotation and peak drift demand of columns is increased compared to the ordinary and intermediate ones. The maximum differences in plastic rotation and peak drift demand between ordinary and special frames were obtained as approximately 70% and 50% in base-isolated buildings.

E-ISSN: 2345-4423

© 2025 The Authors. Journal of Rehabilitation in Civil Engineering published by Semnan University Press.

This is an open access article under the CC-BY 4.0 license. (<https://creativecommons.org/licenses/by/4.0/>)

How to cite this article:

Razavian Amrei, S. A., Ahmadi, S. A., Shakouri, A., Ghodrati Amiri, G. and Rajabi, E. (2026). Effect of Ductility Level on the Seismic Behavior of Low Reinforced Concrete Moment-Resisting Frames Equipped by Double Friction Pendulum Bearings Isolation. *Journal of Rehabilitation in Civil Engineering*, 14(1), 2107 <https://doi.org/10.22075/jrce.2025.34278.2107>

1. Introduction

Severe natural threats with low probability are significantly threatening for economic stability and public safety. In order to decrease the direct/indirect damage caused by these natural disasters, various design approaches and management strategies have been presented in the technical literature of structures and earthquakes [1–3]. Since the strong ground motions are considered one of the greatly catastrophic natural threats, scholars have proposed a variety of design methods for different buildings for reducing earthquake damage [4–8]. From the perspective of researchers, base isolation is one of the most appropriate approaches among design methods for controlling or protection of buildings and other structures from severe damage of strong ground motions. This method is mainly based on the idea of separating structures from lateral motions of earthquakes, which considerably reduces forces induced by earthquake and enhances the seismic behavior of structures [9]. Seismic isolation relies on a flexible device mounted on the base of structures to elongate the natural period of the structures to the low-acceleration region of the design spectrum. Therefore, less design forces elastically are dedicated to an isolated building, leading to elimination or reduction of structural damage in comparison to conventional building (with fixed base) with inelastic response-based design. Furthermore, enhanced protection of nonstructural components, building contents, and augmented energy dissipation and/or re-centering capability will be feasible in isolated structures through lower floor accelerations [10,11]. There are many isolated structures designed and evaluated based on the ASCE/SEI 7-10 [12] and ASCE/SEI 7-16 [13] requirements. According to the superstructures' lateral force-resisting system, these standards suggested R-factors ranging between 1.0 and 2.0. The superstructure must be designed considering all relevant requirements for non-isolated structures [12]. However, it is possible also to select the conventional steel ordinary concentrically braced frames for the superstructure [13]. Substantial structural participation in the first modes of the isolated structures is obtained through the flexibility of the moment-resisting frames [14]. Thus, the following issues are raised:

- (1) Can ordinary and intermediate RC isolated moment-resisting frames exhibit acceptable performance in severe earthquakes?
- (2) In terms of seismic responses, e.g., peak story drift, peak floor acceleration, base shear, and plastic rotation of elements, what are the achievements of isolated structures with varying ductility levels in the superstructure?

Although the isolated moment-resisting frames with varying levels of ductility have somewhat different R-factors, the frames are designed according to the various requirements, including joint shear strength. Therefore, it seems essential to evaluate their seismic responses. The answers of the above mentioned questions can be achieved in some studies [15–19]. A key result for an isolated building in these studies is that accumulation of the ductility demands in the superstructure on yielding is quicker than a similar fixed-base structure [14]. For improving the seismic functioning of vital structures, e.g., hospitals, base-isolation systems should be considered in their design [20]. Consequently, the seismic susceptibility of isolated and fixed hospitals was evaluated by Mazza et al. [21] and shaking tables and numerical tests were compared. This study aimed to evaluate a hospital setting, focusing specifically on assessing and categorizing the functionality of essential medical equipment and nonstructural components. To this end, two scaled models were developed with isolated and fixed bases – representing the hospital structure- and shaking table tests were applied at the University of Kyoto. The conventional laminated elastomeric bearing isolators are used as efficient technologies in protection of civil structures against earthquake. However, they generally have large sizes and are heavy and costly. Thus, Ghorbi and Toopchi-Nezhad presented a modern hollow circular (HC) fiber-reinforced elastomeric isolators for lightweight structures by [22]. They introduced a preliminary design and analytical investigation of isolators. According to

research findings, lighter weight and lower material volume of the HC isolator brings about economic advantages. Unreinforced masonry (URM) structures are among highly vulnerable buildings in earthquakes. Losanno et al. [23] examined the seismic fragility of base-isolated URM structures supplied with recycled and classical rubber bearings in Himalayan regions. They reported a considerable decline in vulnerability of isolated models. Moreover, recycled-rubber fiber-reinforced elastomeric isolators show superior performance compared to classical laminated rubber bearings. Belbachir et al. studied improved response of residential RC structures equipped by an innovative base isolation methodology [24]. They examined the influence of Fluid Viscous Dampers (FVDs) on the process of changing seismic responses of a short isolated residential RC structure by high-damping rubber bearings. This study offers valuable insights for engineers regarding construction of resilient structures in the seismically active zones. Ding et al. [25] studied the inelastic and elastic seismic response of non-structural elements of 3, 5, and 7 story steel moment framed under a wide range of far- and near-field ground motions. In our study, some relations were presented to anticipate the inelastic displacement ratios based on the results of sensitivity to viscous damping and strain hardening. Kasai and Chimamphant [26] compared the seismic behavior of nonstructural elements in isolated structures and fixed-based buildings. It was claimed that isolated structures with longer period exhibit less floor acceleration and drift ratios.

Nie et al. examined dynamic properties and seismic functioning of a single-layer cylindrical grid shell structure [27]. For this purpose, they considered different seismic isolation layouts involving the establishment of layered rubber bearings and new 3D isolation bearings. Considering that extended-duration velocity pulses result in unpredicted seismic demands of isolated structures, Sreeman and Roy [28] investigated the performance of isolated structures with a shape memory alloy-based friction pendulum system (FPS) subjected to near-fault earthquakes. This study showed that the optimal shape memory alloy-based FPS causes an essential decline in the bearing displacement in comparison to the FPS. The collapse of isolated structures in comparison to fixed base ones was evaluated by Kitayama and Constantinou [29]. A 2D 6-story steel model was employed to assess the seismic collapse functioning in fixed and isolated structures with steel Special Moment-Resisting Frame (SMRF), Special Concentric Brace Frame (SCBF), and Ordinary Concentric Brace Frame (OCBF) lateral-resisting systems. For constant behavior coefficient (R), it was shown that the probability of collapse reduces with increment of displacement capacity. Zhang et al. (2023) implemented three-layer isolation systems in elevated buildings and evaluated their seismic response [30]. They demonstrated that the triple-layer isolation device in the studied shear structures outperforms the double-layer and single-story isolation devices under rare earthquakes. Moreover, many studies have assessed 2D models for the seismic performance evaluation [26–29]. 3D models are needed because 2D models cannot provide a precise description of the actual behavior of isolated buildings. Furthermore, the requirements of the previous version of [13] have been used for designing the isolated structures in various studies. However, since these codes have been developed during recent years, there are a few comparative evaluations on isolated RC moment-resisting frames that have been designed based on [13].

It seems that a comparative 3D investigation is required to examine seismic behavior of isolated and fixed RC moment-resisting structures considering different ductility levels. DFPB is selected for assessing seismic behavior of isolated and fixed structures, as proposed by different scholars. DFPB is an enhanced version of the FPS that has been extensively employed in recent periods because of the suitable seismic functioning [31]. Despite introduction of new generation of friction pendulum bearings to the literature for attaining high energy dissipation capacity, it is still required for carrying out a more complete investigation on DFPB. In our work, the impact of ductility level on the seismic behavior of isolated and fixed structures containing RC moment-resisting frames is evaluated using nonlinear dynamic analysis. Hence, three story RC models with fixed and isolated bases and considering ordinary, intermediate, and special ductility are designed. 3D models are implemented in Open Sees software [32] that is appropriate

finite element software for numerical analysis. These models (6 cases) are assessed under 20 pairs of strong ground motion records with 2475-year return periods, which have been scaled based on [13].

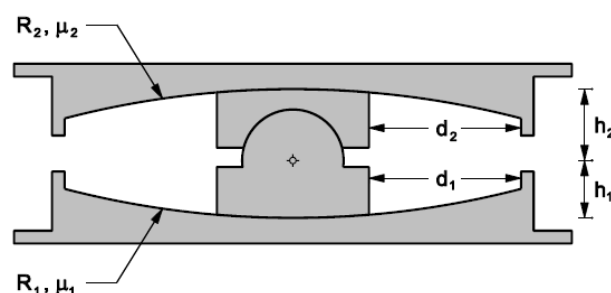
After determination of the response spectrum (with 5% damping) for isolated buildings, the Square Root of Sum of Squares (SRSS) was computed for response spectrum for two horizontal components. Seismic scenarios were scaled to align with the target spectrum within the interest period range, defined from $0.75T_M$ (based on the upper bound) to $1.25T_M$ (based on the lower bound isolation system features). For periods within this range, the average of 20 SRSS combinations was greater than or equal to the Risk-Targeted Maximum Considered Earthquake (MCE_R) spectrum. For the conventional structures, the maximum of the two horizontal components was considered instead of SRSS. Thus, a maximum-direction spectrum extracted based on two horizontal components of ground motion for each pair. Based on the same scale factor, which has utilized for two horizontal components, ground motions are scaled so that the average of the maximum-direction spectra from all scenarios equals or greater than the target response spectrum in the period span of $0.2T$ to $2.0T$ (T = the maximum fundamental period of structure), which should consist the periods needed for more than 90% mass participation in two directions of the structure. For periods within the specified range, the average of 20 spectra is greater than 0.9 times the MCE_R spectrum [13]. Table 1 reports the scale factors for ground motions. Seismic responses of studied models are calculated in terms of base shear, plastic rotation of columns, maximum floor acceleration, and peak story drift.

Table 1. The scale factors of the strong ground motions.

Building		Scale factor
Conventional	OMRF	1.0000
	IMRF	1.0000
	SMRF	1.0000
Base-isolated	OMRF	1.0010
	IMRF	1.0010
	SMRF	1.0373

2. A brief review of DFPB

DFPB has a joint slider sliding on two steel spherical surfaces. Low-friction materials, such as Polytetrafluoroethylene (PTFE), coat the slider. This material can slide on the spherical surface [31]. The sliding system usually presents changes in its response in two major phases: (1) the phase of sticking, and (2) the phase of sliding. In first phase, one or both velocity components are very low or zero, while motion starts in both directions in the second phase. Sliding begins at the primary movement of the sliding reversals and isolator (stick–slip phase), and extent of the static friction coefficient related to these instances is considerably greater than the extent when the isolator slides [33]. The capacity for enduring greater horizontal displacement is the main advantage of DFPB over the isolator with a single friction pendulum (SFPB). It is a system containing two plates at the bottom and top of the stainless steel, with the bottom plate having a radius of curvature, R_1 and the coefficient of friction, μ_1 , and the top plate having a radius of curvature, R_2 and the coefficient of friction, μ_2 (Fig. 1).



(a)

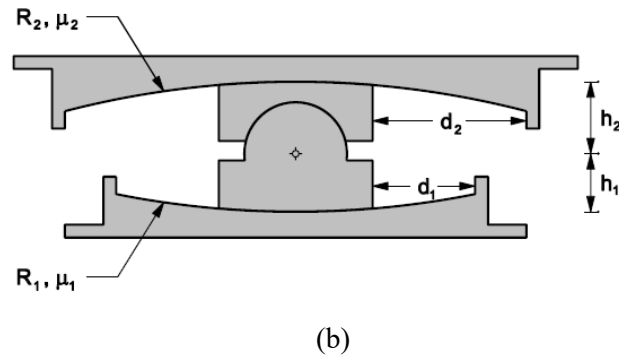


Fig. 1. Double friction pendulum bearing (a) identical plates, (b) non-identical plates [31].

The distribution and cost of displacement between sliders were decreased by using a similar coefficient of friction for two plates. The overall behavior of the isolator is due to the combination of two different slides on two different surfaces, where the sliding order has an important impact on the overall performance. The hysteresis curve of this isolator includes three steps.

Step 1: No motion occurs until the lateral force is less than the isolator plates’ friction force. As the lateral force increases and reaches the plate’s friction force with a smaller friction coefficient, the slide at this plate will begin.

Step 2: As the lateral force increases and attains the friction force of the plate with a larger friction coefficient, the second plate displacement begins. At this moment, displacement has reached a certain amount. With the onset of the second phase and increasing displacement, the slide occurred simultaneously on the two plates and this phase stops when the slider touches the displacement retainer of each plate.

Step 3: Third phase starts after the slider meets the displacement retainer, and the slide only occurs at the plate where the slider has not hit its displacement retainer. At this phase, loading of the first plate with a lower friction coefficient may occur before loading of the second plate with a higher friction coefficient (Phase III(a) in Fig. (2) or vice versa (Phase III (b) in Figure (2)). In the present study, DFPB with similar friction coefficient and radius for two plates are used.

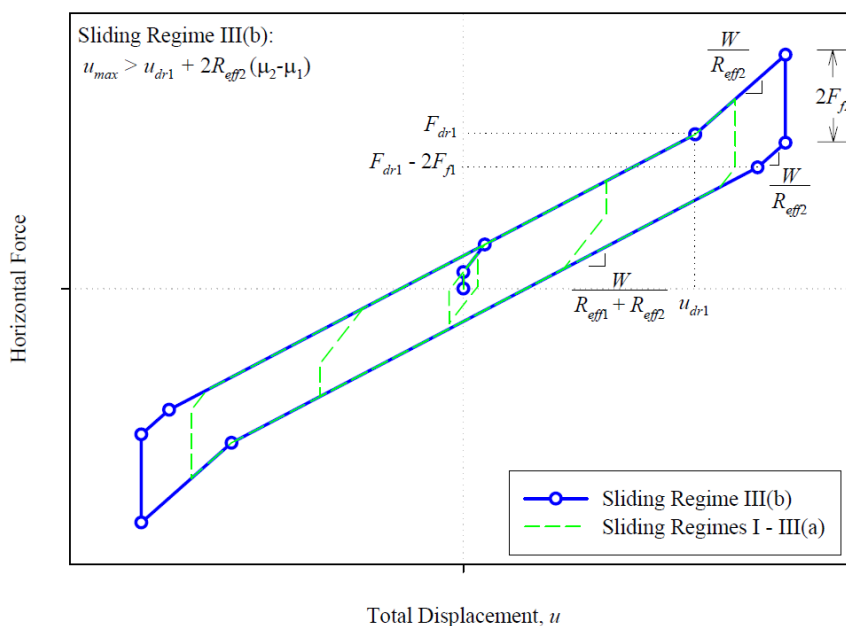


Fig. 2. Hysteresis curve of double friction pendulum bearing in three different steps [31].

3. Studied models

3.1. Design of the studied buildings

In this paper, we considered three story buildings, which had been assessed in the NEES-TIPS project [34], with the difference that the RC moment resisting system was selected for all frames. The length of spans and height of stories were reduced according to Fig. 3. It should be noted that this building has been used in different studies, e.g., [10,14,35,36]. Six models with isolated and fixed bases were developed in accordance with ASCE/SEI 7-16 [13] and ACI 318-14 requirements, and the intermediate, special, and ordinary ductility levels were considered.

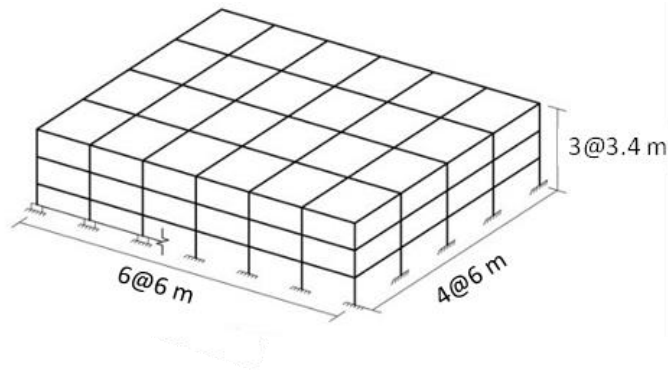


Fig. 3. Visual schematic of the studied buildings with fixed and isolated bases: 3D view.

Since these office models were in Los Angeles, California (Longitude -118.25, Latitude 34.05), D class of soil, importance factor equal one ($I=1.0$), and second occupancy category were considered. For this location, spectral acceleration at period of 1s (S_1) and short periods (S_s) are 0.703g and 1.974g, according to the USGS site [37] (g denotes gravity acceleration). The site coefficient values were assumed as $F_a = 1$ and $F_v = 1.7$. The concrete's compressive strength was considered 28MPa, and the reinforcement type was assumed as A615G40 with the yield strength of 340MPa and the ultimate strength of 500MPa. Table 2 presents the structures' response modification factors. The allowable story drift was considered 1.5% and 2.5% of story height for buildings with isolated and fixed bases, respectively. For the isolation system, Double Friction Pendulum Bearings were used. The isolation systems and base-isolated structures were designed using an iterative process [38].

Table 2. Response modification factors.

Building		Response modification coefficient (R)
Conventional	OMRF	3
	IMRF	5
	SMRF	8
Base-isolated	OMRF	1.125
	IMRF	1.875
	SMRF	2

The procedure presented by Constantinou et al. [39] was used to calculate upper and lower limits of μ (the friction coefficient of plates of isolators). Based on Eq. 1, the maximum isolation system displacement is calculated at the rigidity centre at the MCE_R spectrum (D_M):

$$D_M = \frac{gS_{M1}T_M}{4\pi^2\beta_M} \quad (1)$$

Where $S_{M1} = 1(s)$; $T_M =$ effective isolation period; $\beta_M =$ modification coefficient of spectrum for damping. The total maximum D_M at MCE_R spectrum (D_{TM}), including the displacement caused by accidental and actual torsion, was obtained based on Eq. 2:

$$D_{TM} = D_M \left[1 + \left(\frac{y}{P_T^2} \right) \frac{12e}{b^2 + d^2} \right] \quad (2)$$

Where y denotes the space between the rigidity centres of all isolators and the particular element vertical to the direction of the studied seismic loading [in. (mm)]; e is considered as the sum of the measured actual and accidental eccentricity in plan between the centre of the structure mass above the isolation level and the rigidity centre of the isolation system; b and d are dimension of plan; P_T is the effective ratio of the translational to torsional period of the isolation system. Equations 3-5 were used to obtain the minimum lateral seismic force to design structural components under the level of the base, isolation system, and foundation (V_b), and the minimum and unreduced lateral seismic design force for structural components beyond the base level (V_{st} and V_s):

$$V_b = k_M D_M \quad (3)$$

$$V_s = \frac{V_{st}}{R_I} \quad (4)$$

$$V_{st} = V_b \left(\frac{W_s}{W} \right)^{(1-2.5\beta_M)} \quad (5)$$

Where W_s shows the structure's effective structural seismic weight beyond the isolators, except the effective seismic weight of the base level; k_M denotes the effective stiffness of the isolation system at D_M ; R_I is the superstructure's response modification factor; β_M is the effective damping, and W is the effective structural seismic weight above the isolators. Columns and beams of the case studies were designed based on the distributed minimum lateral seismic design force over the structure's height above the base level. Parapet and wall dead load were 4.81 and 3.92 kPa, respectively. Dead and live loads were 2.55 and 0.96 kPa for roof. Live and dead loads were 2.4 and 2.01 kPa for other floors. The floors were composite with metal decks. Partitions live load and snow load were 1.45 and 0.23 kPa. The effective seismic weights of structures and the final section of structural components are presented in Tables 3 and 4. Figure 4 presents the columns' reinforcement details. Table 5 presents the final design values of base-isolated buildings and isolation systems.

Table 3. Effective seismic weight of the fixed and isolated models.

Building		Effective seismic weight (kN)				Total
		Base level	First floor	Second floor	Third floor (roof)	
Fixed-base	OMRF	—	11354.78	9688.79	6165.95	27209.52
	IMRF	—	9968.87	10057.05	6165.95	26191.87
	SMRF	—	8620.62	8476.71	4970.99	22068.32
Isolated	OMRF	9095.1	9445.79	7640.22	4970.99	31152.11
	IMRF	8977.66	9118.64	7584.56	4881.01	30561.88
	SMRF	8105.79	8319.43	7130.2	4483.84	28039.26

Table 4. Final cross sections of structural components.

Sections of the beams and columns	Fixed-base building			Isolated building			
	OMRF	IMRF	SMRF	OMRF	IMRF	SMRF	
Base level	Beams in x-direction	—	—	—	B50x45cm	B50x50cm	B45x40cm
	Beams in y-direction	—	—	—	B50x50cm	B50x50cm	B45x45cm
First floor	Beams in x-direction	B60x60cm	B55x50cm	B45x45cm	B50x45cm	B50x50cm	B45x40cm
	Beams in y-direction	B60x60	B55x50	B45x45	B50x50	B50x50	B45x45
	Columns	C65x65cm (28Φ28)	C55x55cm (20Φ28)	C45x45cm (16Φ25)	C60x60cm (24Φ28)	C50x50cm (20Φ28)	C50x50cm (20Φ28)
Second floor	Beams in x-direction	B55x50cm	B55x55cm	B45x45cm	B35x35cm	B40x40cm	B35x35cm
	Beams in y-direction	B55x50cm	B55x55cm	B45x45cm	B40x40cm	B40x40cm	B40x35cm
	Columns	C55x55cm (20Φ28)	C55x55cm (20Φ28)	C50x50cm (20Φ28)	C50x50cm (20Φ28)	C40x40cm (12Φ25)	C40x40cm (12Φ25)
Third floor (roof)	Beams in x-direction	B45x45cm	B45x45cm	B35x35cm	B35x35cm	B35x35cm	B30x30cm
	Beams in y-direction	B45x45cm	B45x45cm	B35x35cm	B35x35cm	B35x35cm	B35x30cm
	Columns	C45x45cm (16Φ25)	C45x45cm (16Φ25)	C40x40cm (12Φ25)	C40x40cm (12Φ25)	C35x35cm (12Φ25)	C30x30cm (8Φ25), C35x35cm (12Φ25)

Despite some uncertainties, finite element (FE) modelling is still known as a robust instrument to evaluate the behaviour of structural elements under different loading conditions [40–42], the 3D-models of six structures were implemented in Open Sees software [43]. The mass of stories was concentrated in the centre of mass. Rigid diaphragm constraint was considered for slabs and modelled with the “rigid Diaphragm” [32] command in the software.

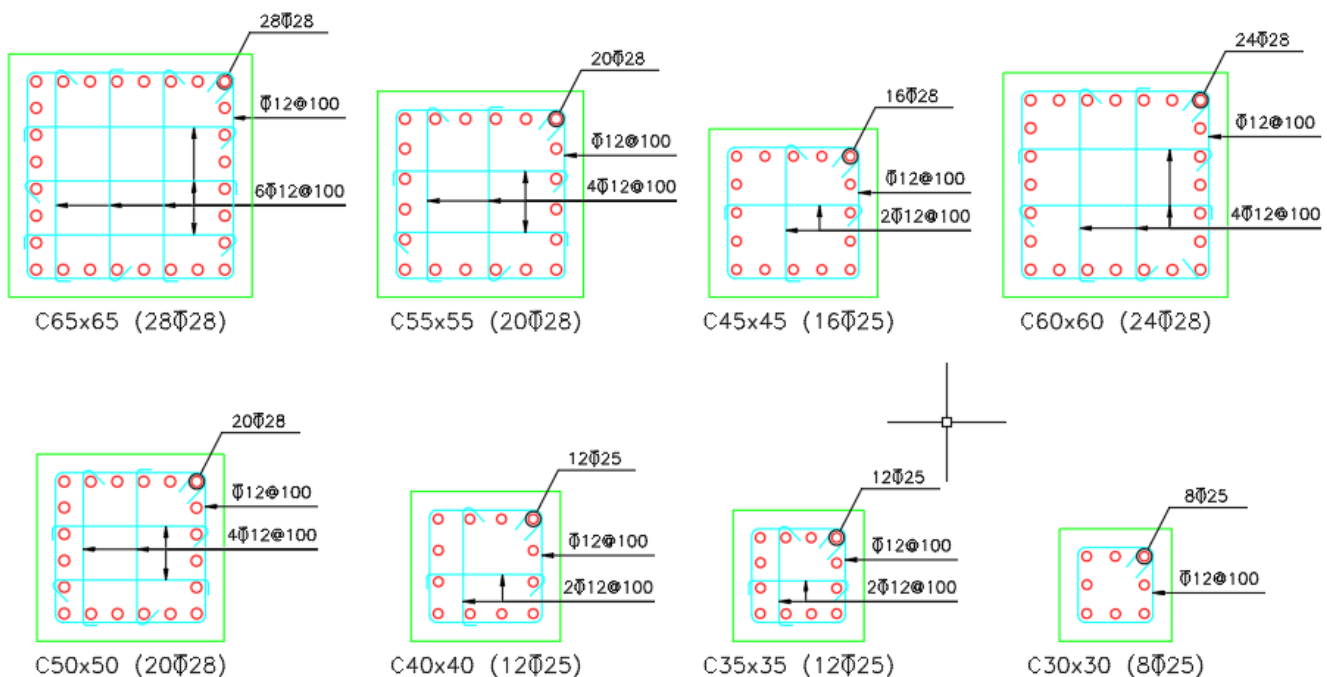


Fig. 4. Reinforcement details of columns.

Table 5. Summary of design of isolated buildings and isolation systems.

Parameter	OMRF		IMRF		SMRF		Unit
	Lower bound	Upper bound	Lower bound	Upper bound	Lower bound	Upper bound	
μ	0.0685	0.1148	0.065	0.1153	0.07	0.1176	—
D_M	0.61	0.45	0.62	0.45	0.64	0.47	m
R_{eff}	2	2	2	2	2.6	2.6	m
k_M	19074.28	23523.3	18485	23111.57	13851.12	17800.11	$\frac{\text{kN}}{\text{m}}$
T_M	2.564	2.309	2.58	2.307	2.855	2.518	s
β_M	0.1168	0.2151	0.1103	0.2157	0.141	0.2509	%
D_{TM}	0.7015	0.5175	0.713	0.5175	0.736	0.5405	m

The material “Concrete01” [32] was used for the modelling of concrete, and “ReinforcingSteel” was employed for rebar [44–46]. The rebar’s ultimate strength and yield strength were considered 500 and 340 MPa. Force-based nonlinear beam-column element "element forceBeamColumn" with five integration points as distributed plasticity was selected for implementation of all beams and columns. Similar to [47,48], the rectangular sections with fibre sections were designated for columns and beams in all models, which considered the relations between moment and axial force at every analysis step. Rayleigh damping [49] was used for all buildings. Rayleigh damping is calculated by Eq. 6:

$$c = \alpha_M[M] + \beta_k[K_{current}] + \beta_{Kinit}[K_{init}] + \beta_{Kcomm}[K_{lastcommit}] \quad (6)$$

Where $[M]$, $[K_{current}]$, $[K_{init}]$, and $[K_{lastcommit}]$ are the mass matrix, current stiffness matrix, initial stiffness matrix, and last committed stiffness matrix, respectively, and α_M , β_k , β_{Kinit} , and β_{Kcomm} are the factors of these matrices, respectively, obtained from Eq. 7 and 8.

$$\alpha_M = \frac{2\xi\omega_i\omega_j}{\omega_i + \omega_j} \quad (7)$$

$$\beta = \frac{2\xi}{\omega_i + \omega_j} \quad (8)$$

3.2. Implementation of models

In the current work, β_k and β_{Kcomm} were set to zero. For the first two modes in structures with isolated bases, we set mass proportional term to zero, and only stiffness proportional damping was applied instead of Rayleigh damping [50]. We also used the "integrator Newmark 0.5 0.25" and "algorithm Newton" for nonlinear time history analysis.

3.3. Modeling of isolators

The DFPBs were installed separately beneath each column. The “element single FPBearing” was selected for isolators while torsional, moment direction, and axial direction materials of isolators were considered by “uniaxial Material Elastic” and “uniaxial Material ENT” (Elastic, no Tension), respectively [32]. For modeling of isolators, a “Zero Length element” was described between two nodes with the same coordinates described beneath each column. Among different types of coefficients of friction for the frictional isolators (velocity dependent, axial and velocity force dependent, constant, pressure and velocity-dependent and multi-linear velocity), the velocity dependent case was selected and assigned by “frictionModelVelDependent” [32], which can be calculated based on Eq. 9 [51]:

$$\mu = \mu_{fast} - (\mu_{fast} - \mu_{slow}) \cdot e^{-a\dot{u}} \quad (9)$$

Where \dot{u} = velocity at the sliding interface; a = a rate parameter; μ_{fast} and μ_{slow} and = friction coefficient at a fast and slow velocity. The above parameters were considered in the current study:

$$\mu_{fast} = \mu \qquad \mu_{slow} = 0.5\mu \qquad a = 250 \frac{s}{m}$$

In the above parameters, μ denotes the friction coefficient calculated from designing isolation systems. The results of the experiment presented in [31] were employed to validate the model used for the DFPBs. The characteristics and configuration of the experiment were modelled analytically. Fig. 5 compares the results of our analytical modelling with the experimental research, showing a good fit. Table 6 presents the elements used in OpenSees for modelling both fixed-base and isolated buildings.

4. Seismic scenarios

20 pairs of strong ground records were obtained from the PEER center for conducting nonlinear time history analysis [52]. The selected records had magnitude range of 6-7.35 (Table 7) for soil class D. In addition to two horizontal elements of the records, vertical element was employed for analysis, according to [13]. These pairs of horizontal ground motions are identical to records employed in NEES-TIPS project [34], which were scaled to the MCE_R spectrum of [13] in the current work. The amplitude method was applied for scaling selected records of ground motion [13].

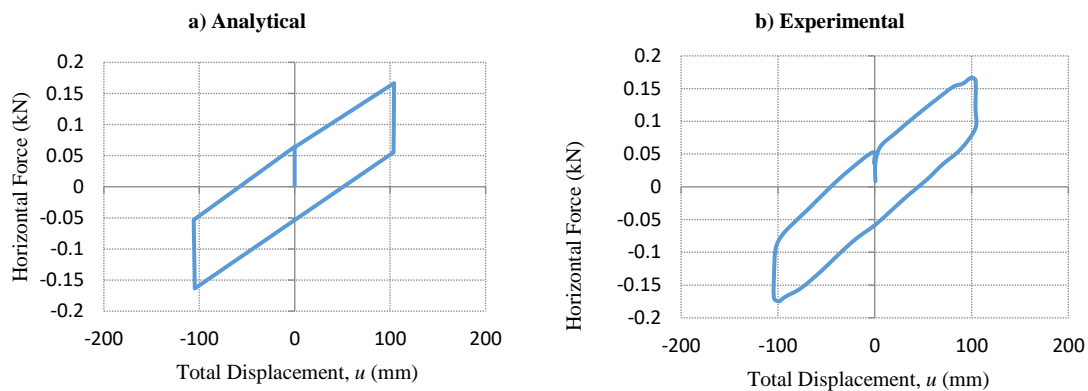


Fig. 5. Validation of DFPB modeling, (a) Our results, (b) Results from [31].

Table 6. Elements utilized in Open Sees.

No.	Open Sees Element	Discription
1	rigid Diaphragm	Rigid Diaphragm
2	Concrete01	Concrete Material
3	Reinforcing Steel	Rebar Material
4	element force Beam Column	Concrete Beam and Column
5	element singleFPBearing	FPB Element
6	uniaxial Material Elastic	FPB Material in Moment Direction
7	uniaxial Material ENT	FPB Material in Axial Direction
8	frictionModelVelDependent	Coefficient of Friction of FPBs

The response spectrum with 5% damping was calculated for isolated models using normalized components. In the following, the SRSS of response spectrum was determined for horizontal elements. With scaling the seismic scenarios, an MCE_R was met in the desired range of period, which was specified as $0.75T_M$. It was computed by upper limit of characteristics of isolator to $1.25T_M$ from their lower bound [38]. For these periods, the average of 20 SRSS of records was greater than one time the MCE_R spectrum. The maximum horizontal component is applied rather than SRSS in the conventional structures. Fig. 6 shows the earthquakes' mean spectrum in comparison to the standard spectrum.

5. Results of nonlinear dynamic analysis

We carried out the nonlinear time history analysis for all studied models under 20 pairs of ground motion records. For each desired seismic result, related parameters, such as the peak story drifts at the corner of story, the peak floor accelerations at the center of mass, the base shear of the buildings and the plastic rotation of columns, and the maximum values were determined, and the average values were given for the buildings. Since many seismic responses were obtained from nonlinear dynamic analysis, the 84th percentile was utilized to obtain seismic responses along with the average values. The 84th percentile was described as $\bar{x} + \sigma$ where \bar{x} , and σ were mean and SD, respectively and determined by Eq. 10 and 11 [14].

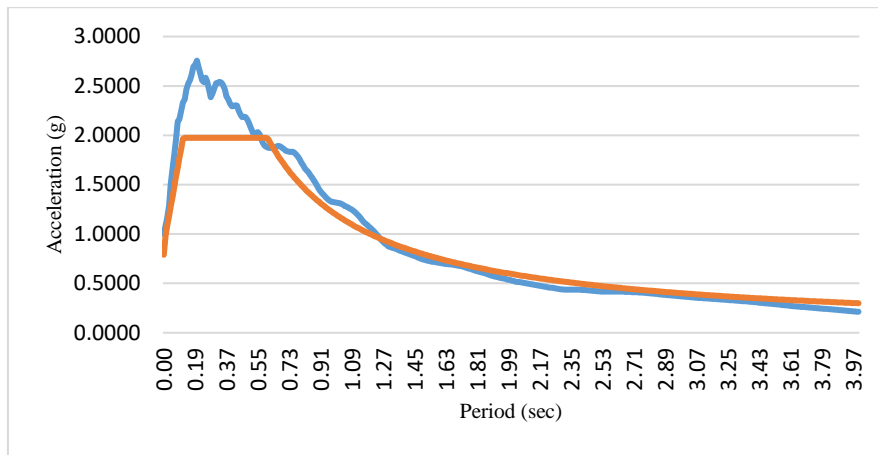
$$\bar{x} = \frac{\sum_{i=1}^n x_i}{n} \quad (10)$$

$$\sigma = \sqrt{\frac{\sum_{i=1}^n (x_i - \bar{x})^2}{n-1}} \quad (11)$$

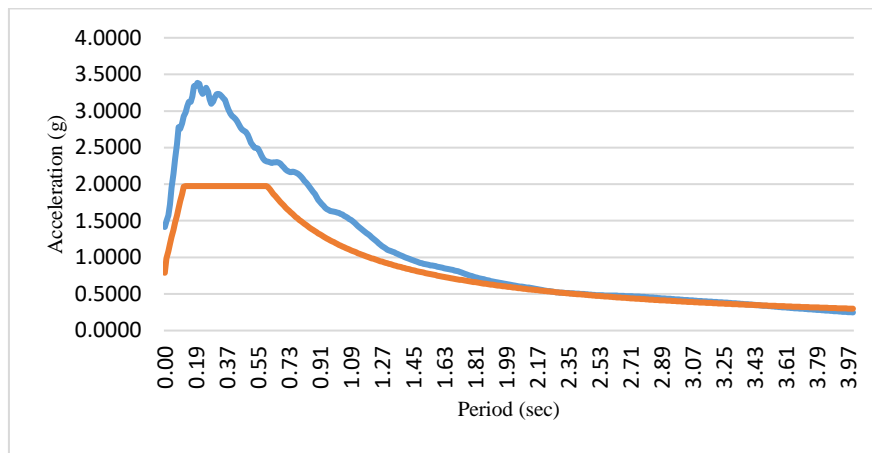
Figures 7, 8, and 9 indicate the time history graphs for Kobe earthquake.

Table 7. Characteristics of pairs of horizontal ground motion.

No	Name	Year	Station	M	Mechanism	R_{jb} (km)	R_{rup} (km)	V_{S30} ($\frac{m}{s}$)
1	Tabas, Iran	1978	Dayhook	7.35	Reverse	0	13.94	471.53
2	Imperial Valley-06	1979	Cerro Prieto	6.53	strike slip	15.19	15.19	471.53
3	San Salvador	1986	Geotech Investig Center	5.8	strike slip	2.14	6.3	489.34
4	San Salvador	1986	National Geographical Inst	5.8	strike slip	3.71	6.99	455.93
5	Loma Prieta	1989	APEEL 7 – Pulgas	6.93	Reverse Oblique	41.68	41.86	415.27
6	Loma Prieta	1989	BRAN	6.93	Reverse Oblique	3.85	10.72	476.54
7	Loma Prieta	1989	LGPC	6.93	Reverse Oblique	0	3.88	594.83
8	Loma Prieta	1989	Saratoga - Aloha Ave	6.93	Reverse Oblique	7.58	8.5	380.89
9	Loma Prieta	1989	WAHO	6.93	Reverse Oblique	11.03	17.47	388.33
10	Northridge-01	1994	Beverly Hills - 12520 Mulhol	6.69	Reverse	12.39	18.36	545.66
11	Northridge-01	1994	Jensen Filter Plant Administrative Building	6.69	Reverse	0	5.43	373.07
12	Northridge-01	1994	Sunland - Mt Gleason Ave	6.69	Reverse	12.38	13.35	402.16
13	Northridge-01	1994	Sylmar - Converter Sta East	6.69	Reverse	0	5.19	370.52
14	Kobe, Japan	1995	Nishi-Akashi	6.9	strike slip	7.08	7.08	609
15	Duzce, Turkey	1999	Lamont 1058	7.14	strike slip	0.21	0.21	529.18
16	Duzce, Turkey	1999	Lamont 1059	7.14	strike slip	4.17	4.17	551.3
17	Duzce, Turkey	1999	Lamont 1061	7.14	strike slip	11.46	11.46	481
18	Parkfield-02, CA	2004	Parkfield - Cholame 3E	6	strike slip	4.95	5.55	397.36
19	Parkfield-02, CA	2004	Parkfield - Gold Hill 4W	6	strike slip	7.74	8.27	421.2
20	Parkfield-02, CA	2004	Parkfield - Gold Hill 5W	6	strike slip	11.11	11.52	441.37



(a)

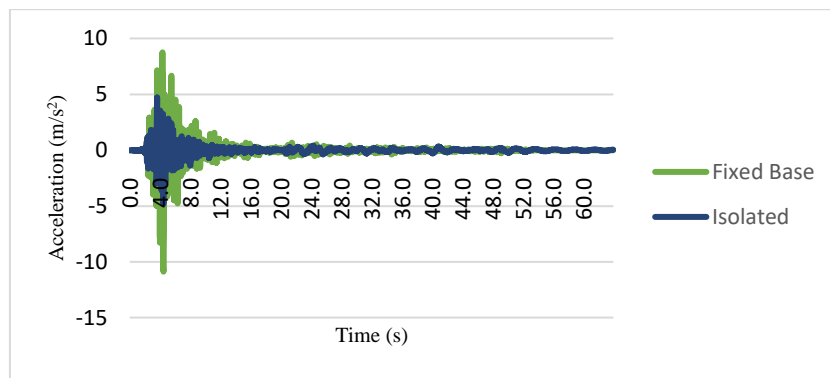


(b)

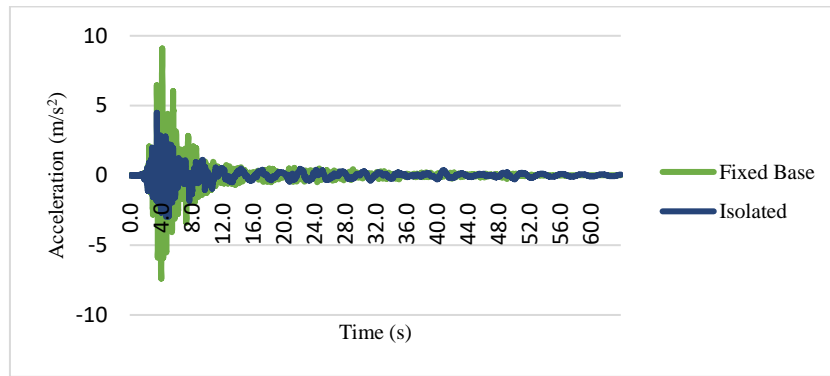
Fig. 6. The mean spectrum of the earthquakes compared to the standard spectrum (a) Fixed-Base Buildings, (b) Isolated Buildings.

5.1. Peak floor accelerations

84th percentile and average of peak floor acceleration are presented in Fig. 10 for three-story buildings. The results show that whether in the average or the 84th percentile in buildings with fixed-base, the peak floor acceleration of the second floor in the OMRF, IMRF, and SMRF structures are nearly equal (OMRF building slightly larger than the other two), but for the first and third floor (roof) the relation for this seismic response is SMRF > IMRF > OMRF, with a slight difference; for example, peak floor accelerations in the x-direction in the first floor are 0.31g and 0.44g in fixed-base OMRF and SMRF, respectively. In the fixed-base models, the peak floor acceleration for different ductility levels increased with the number of stories. However, in the isolated models, the values of peak floor accelerations are approximately equal in all three buildings. The floor acceleration of the isolated models on the 1st floor is greater than that of the fixed-base ones, and lesser on the other floors. The results obtained from the 84th percentile case are nearly 1.5 times those obtained from the average case. The findings imply that the use of isolators has a positive influence on decreasing peak floor accelerations, and this impact elevates with increasing the model’s height, reaching 55% on the third floor. Also, ductility level of superstructure has trivial effect on the floor accelerations in the isolated models. Moreover, the peak floor acceleration in OMRF and IMRF low-rise buildings with isolated base has proper range the same as the SMRF superstructure.

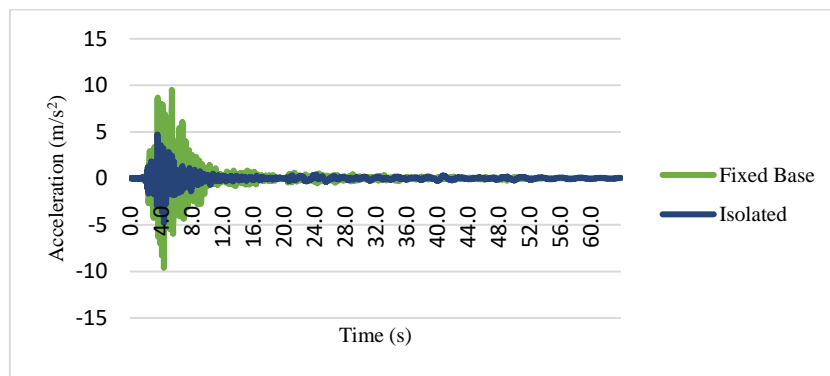


(a)

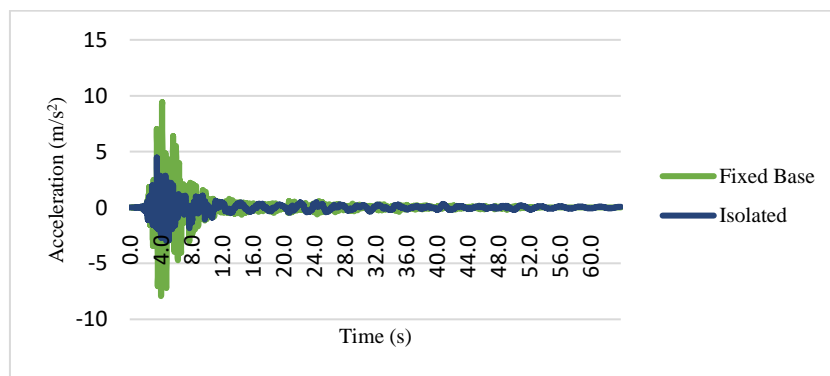


(b)

Fig. 7. Time history graph (a) IMRF buildings in x-direction, (b) IMRF buildings in y-direction.



(a)



(b)

Fig. 8. Time history graph (a) OMRF buildings in x-direction, (b) OMRF buildings in y-direction.

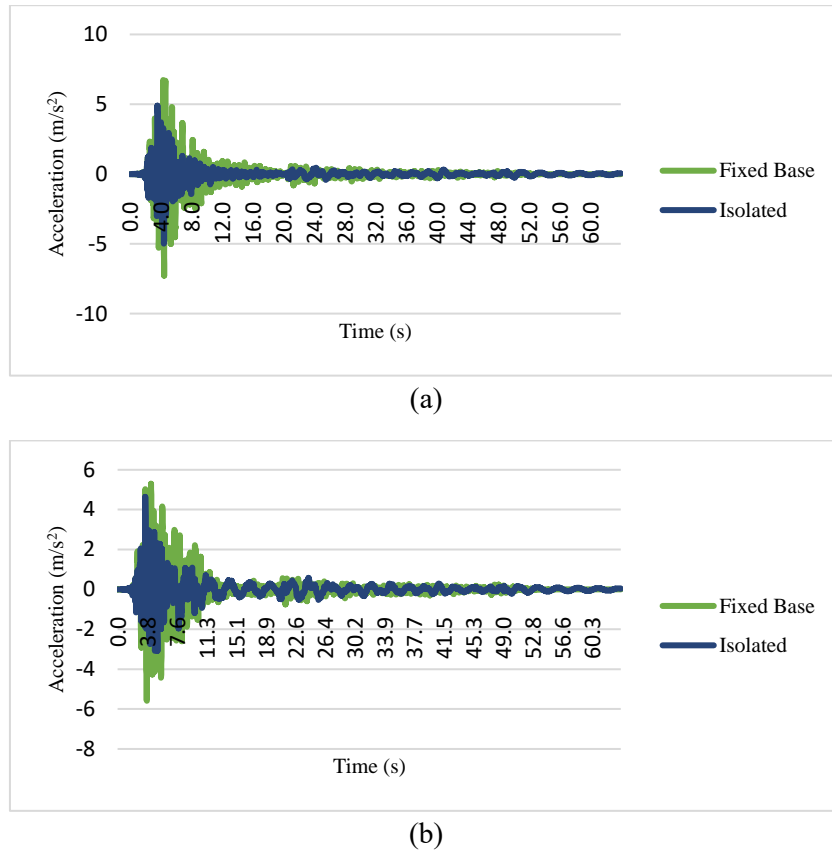


Fig. 9. Time history graph (a) SMRF buildings in x-direction, (b) SMRF buildings in y-direction.

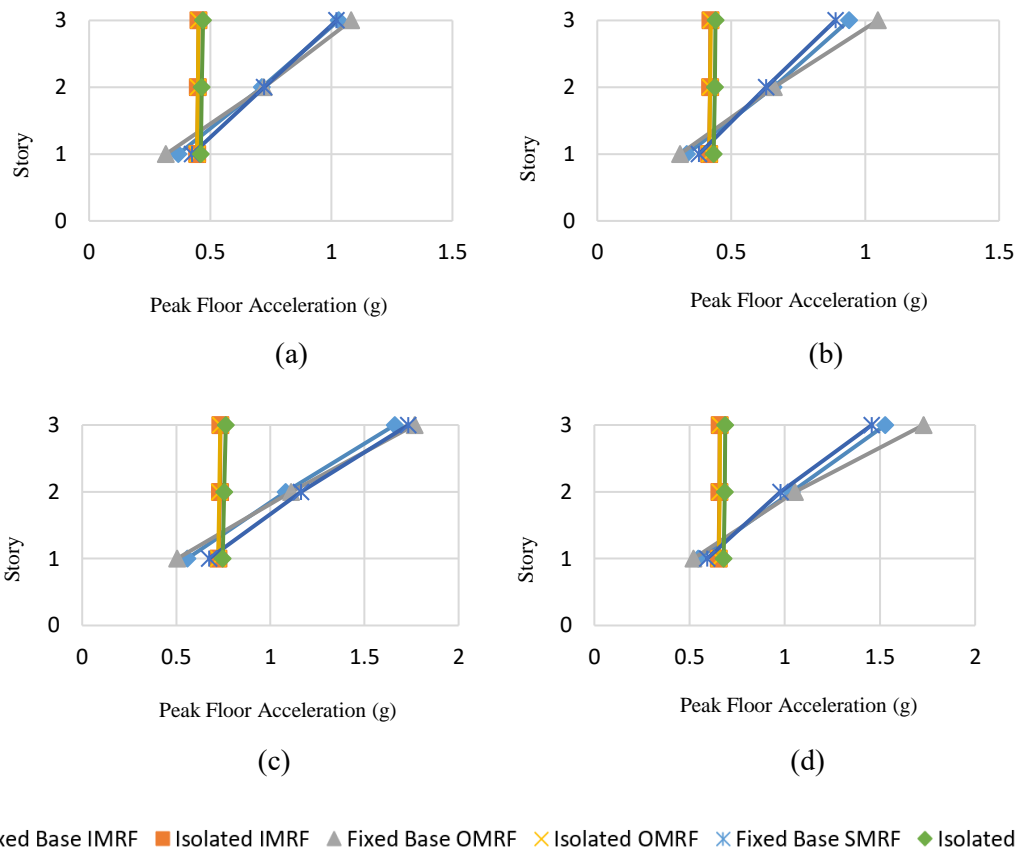


Fig. 10. Peak floor acceleration (a) average in x-direction, (b) average in y-direction, (c) 84th percentile in the x-direction, and (d) 84th percentile in the y-direction.

5.2. Peak ratio of drifts

The peak drift ratio of stories was determined by the nonlinear time history analysis. Then, the average and 84th percentile values were calculated for the models and reported in Fig. 11. The results show that the relation of peak drift ratio for different levels of ductility is as SMRF > IMRF > OMRF in the fixed-base buildings; for instance, peak average drift ratios in the x-direction in the first floor are 0.21% and 0.69% in fixed-base OMRF and SMRF, respectively.

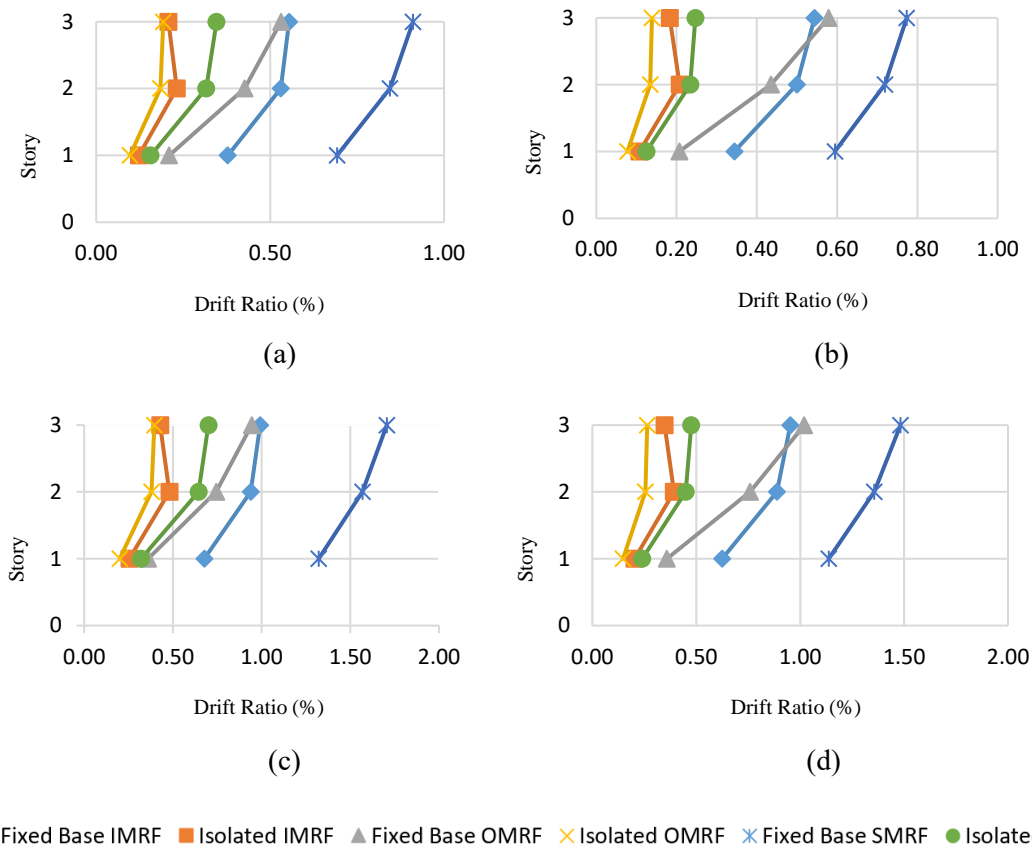


Fig. 11. Peak drift ratio (a) average in x-direction, (b) average in y-direction, (c) 84th percentile in x-direction, and (d) 84th percentile in y-direction.

In fixed-base models, the difference between peak drift ratios for various ductility levels decreased with the number of stories. The maximum drift ratio of IMRF and SMRF models are about 100% and 220% larger than the OMRF building at the first floor, respectively (the maximum difference in both direction), while these values are 25% and 100% at second floor. The drift ratio of the third floor (roof) in the OMRF and IMRF buildings is approximately equal and about 40% lower than the SMRF building. In buildings with isolated bases, this seismic response in the third floor of IMRF and OMRF buildings are approximately equal and about 40% smaller than the SMRF building. The relation between the results in the first and second floor of isolated buildings is SMRF > IMRF > OMRF, with the maximum difference as 50% (in y-direction at third floor). The results obtained from the 84th percentile are about two times larger than the average case. The peak drift ratio of structures with isolated base reduced from 49% to 80% in comparison to similar fixed-base structures. Also, the OMRF and IMRF superstructures showed a proper seismic performance, even better than the SMRF superstructure, in the case of peak drift ratio.

5.3. Base shear of the studied models

Figure 12 presents the 84th percentile and average base shear for the studied structures. The average base shear of the OMRF and IMRF buildings are almost equal and about 35% greater than the SMRF structure

for fixed-base buildings in x-direction. However, the base shear of the IMRF and OMRF buildings are about 25% and 40% larger than the SMRF building in y-direction, respectively. However, this seismic response in structures with isolated base in both y- and x-direction is approximately equal for different ductility levels. The results calculated from the 84th percentile are about 1.8 times larger than the average values. As it is observed, employing DFPB isolators has a positive effect (55% to 77%) on reducing the structures' base shear, while the ductility level of superstructure has trivial influence on the base shear in base-isolated low-rise RC buildings. Also, the isolated OMRF and IMRF buildings present an acceptable performance.

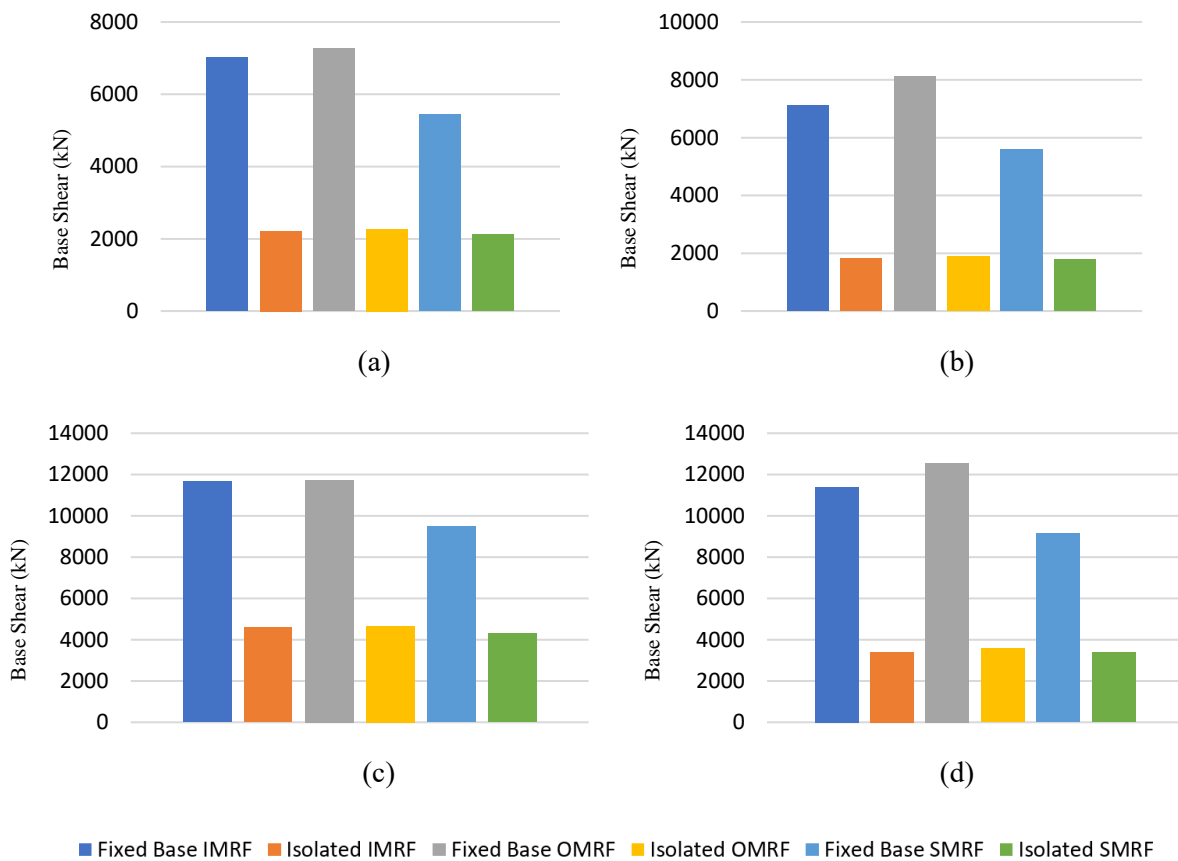


Fig. 12. Base shear (a) average in x-direction, (b) average in y-direction, (c) 84th percentile in x-direction, and (d) 84th percentile in y-direction.

5.4. Plastic rotation of columns

After calculation of the peak plastic rotation of columns, the 84th percentile and average values were determined for the studied models and reported in Fig. 13. The average plastic rotation of columns of conventional buildings for the third floor (roof) of the OMRF and IMRF buildings is about 30% and 40% less than the SMRF, respectively. This response for the second floor in the OMRF and SMRF buildings is approximately equal and about 30% greater than the IMRF building, and in the first floor of the IMRF and OMRF buildings, it is about 50% and 70% less than the SMRF building, respectively. Also, this seismic response in the base-isolated models for the third floor of the IMRF and OMRF buildings is 20% and 65% lower than the SMRF buildings, respectively. For the second floor, the result of IMRF and OMRF buildings is about 10% and 70% less than the SMRF superstructure, respectively, and for the first floor of the three isolated buildings, it is nearly equal. Using DFPB significantly affects the reduction of the plastic rotation of columns, where this effect is higher than 90% in all cases. Even, in some studies, this effect has been reported as about 100%.

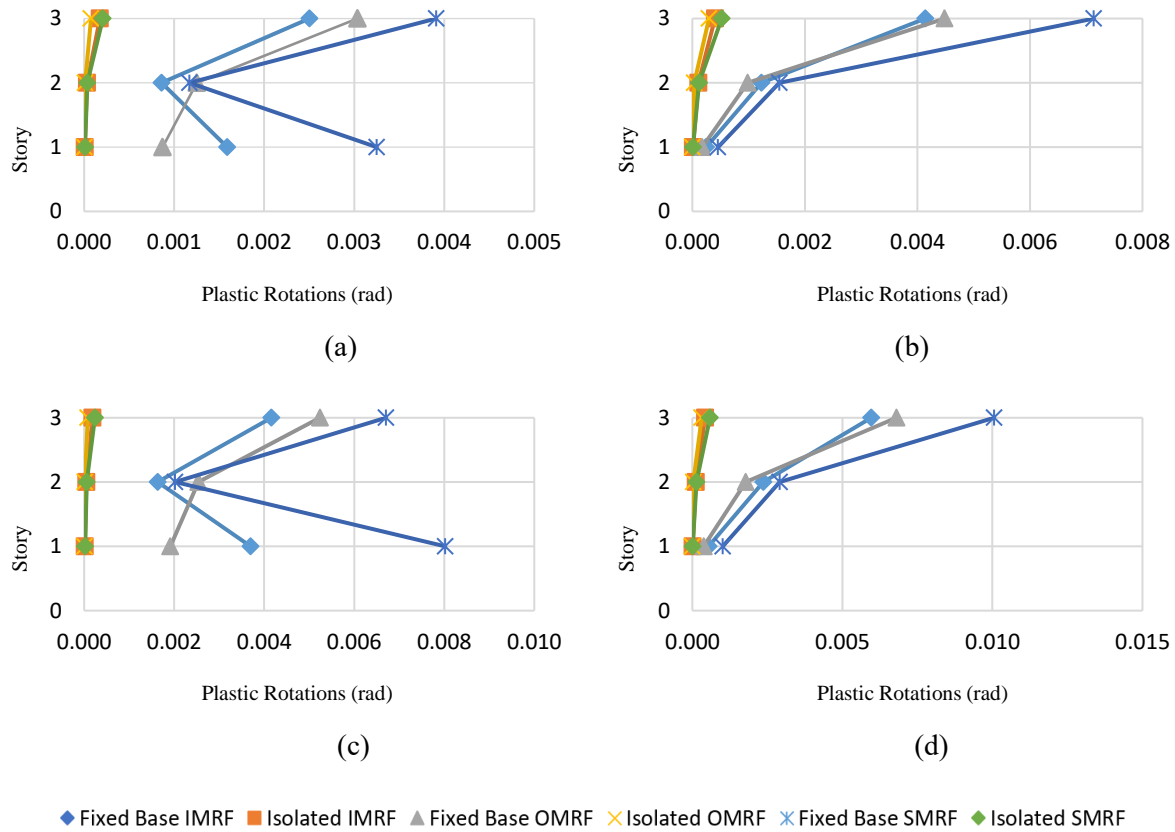


Fig. 13. Plastic rotation of columns (a) average in x-direction, (b) average in y-direction, (c) 84th percentile in x-direction, and (d) 84th percentile in y-direction.

6. Conclusion

In the current work, the impact of ductility levels was reported as a comparative numerical survey on the seismic behavior of isolated and fixed RC moment-resisting frames. To this end, we designed 3D models of the symmetric three-story building, which were implemented in Open Sees software at different ductility levels (ordinary, intermediate, and special). For the isolation system, a DFPB was selected, and 20 pairs of scaled ground motion records were employed for conducting nonlinear dynamic analysis. Seismic responses of models, which include peak floor acceleration, base shear, plastic rotation, and peak story drift of column were calculated and investigated. These conclusions were drawn considering the obtained results:

- The ductility level of the superstructure influences the columns' plastic rotation and peak drift ratio in both fixed and isolated RC moment-resisting frame structures. Peak average drift ratios in x-direction in first floor are 0.21% and 0.69% in fixed-base OMRF and SMRF, respectively. The maximum differences in drift ratio between SMRF and OMRF are 50% and 220% for base-isolated and conventional structures, respectively. The peak difference in plastic rotation of columns is nearly 70% for both kinds of buildings.
- The ductility level slightly influences the base shear and peak floor accelerations of RC moment-resisting base-isolated frames, while it has remarkable effect on conventional structures. Peak average floor accelerations in the x-direction in first floor are 0.31g and 0.44g in the fixed-base OMRF and SMRF, respectively. The maximum difference between SMRF and OMRF is about 40% for the fixed-base buildings.

- Using DFPB has a desirable effect on the seismic responses of RC moment-resisting frame buildings. The most significant decline of peak drift ratio, peak floor acceleration, plastic rotation, and base shear of columns was obtained as about 80%, 55%, 75%, and 100%, respectively.

The ordinary and intermediate low-rise isolated RC moment-resisting frames showed suitable performance for the severe strong ground motions with 2% exceeding in 50 years, the same as the SMRF. The demands fall within an appropriate range and can be reliably predicted for the seismic scenario.

It is worth noting that the modeled buildings are low-rise structures, and utilizing DFPBs in high-rise structures with varying ductility levels will bring different seismic responses. In addition, the effects of shear flexibility in the joint and bar slip have not been considered in this study. Overall, research on the impact of ductility levels on seismic behavior of isolated buildings can be broadened to include various areas, like the use of elastomeric isolators, assessing the influence of building height, and performing analyses to evaluate the collapse performance of these buildings.

Funding

This work did not use any grants from funding organizations in the commercial, public, or not-for-profit sectors.

Conflicts of interest

The authors declared that they have not any competing financial interests or personal relations that could have affected the work presented in this paper.

Authors contribution statement

S. Ali Razavian Amraei: Conceptualization, Investigation, Project administration, Visualization, Supervision.

S. Amirhossein Ahmadi: Data curation, Formal analysis, Investigation, Methodology, Project administration, Resources, Software.

Ayoub Shakouri: Conceptualization, Project administration, Investigation, Visualization, Supervision.

Gholamreza Ghodrati Amiri: Conceptualization, Investigation, Project administration, Visualization, Supervision.

Elham Rajabi: Visualization, Validation, Roles/Writing – original draft, Writing – review & editing, Supervision.

References

- [1] Habib A, Youssefi I, Kunt MM. Identification of pulse-like ground motions using artificial neural network. *Earthq Eng Vib* 2022;21:899–912. <https://doi.org/10.1007/s11803-022-2127-y>.
- [2] Dehcheshmeh EM, Rashed P, Broujerdian V, Shakouri A, Aslani F. Predicting seismic collapse safety of post-fire steel moment frames. *Buildings* 2023;13:1091. <https://doi.org/10.3390/buildings13041091>.
- [3] Rajaei Lak H, Rajabi E, Ghodrati Amiri G, Shakouri A. Numerical Analysis of Regular Reinforced Concrete Frames under Near-Fault Ground Motions. *Iran J Sci Technol Trans Civ Eng* 2023;47:399–414. <https://doi.org/10.1007/s40996-022-00990-y>.

- [4] Amiri GG, Shakouri A, Veismoradi S, Namiranian P. Effect of seismic pounding on buildings isolated by triple friction pendulum bearing. *Earthquakes Struct* 2023;12:35–45. <https://doi.org/10.12989/eas.2017.12.1.035>.
- [5] Habib A, Alnaemi A, Habib M. Developing a framework for integrating blockchain technology into earthquake risk mitigation and disaster management strategies of smart cities. *Smart Sustain Built Environ* 2024. <https://doi.org/10.1108/SASBE-12-2023-0376>.
- [6] Amin Afshar M, Adlparvar MR, Aghaeipour S. Three-Mass Structural-Isolating-Damping Model Subjected to Near-and Far-Fault Earthquakes. *J Rehabil Civ Eng* 2022;10:1–20. <https://doi.org/10.22075/jrce.2021.22466.1482>.
- [7] Babaei S, Zarfam P, Moghadam AS, Zahrai SM. Assessment of a dual isolation system with base and vertical isolation of the upper portion. *Struct Eng Mech An Int'l J* 2023;88:263–71. <https://doi.org/10.12989/sem.2023.88.3.263>.
- [8] Shakouri A, Amiri GG, Miri ZS, Lak HR. Seismic poundings of multi-story buildings isolated by TFPB against moat walls. *Earthquakes Struct* 2021;20:295–307. <https://doi.org/10.12989/eas.2021.20.3.295>.
- [9] Kiliç S, Akbaş B, Shen J, Paolacci F. Seismic behavior of liquid storage tanks with 2D and 3D base isolation systems. *Struct Eng Mech An Int'l J* 2022;83:627–44. <https://doi.org/10.12989/sem.2022.83.5.627>.
- [10] Erduran E, Dao ND, Ryan KL. Comparative response assessment of minimally compliant low-rise conventional and base-isolated steel frames. *Earthq Eng & Struct Dyn* 2011;40:1123–41. <https://doi.org/10.1002/eqe.1078>.
- [11] Habib A, Yildirim U. Modeling reinforced concrete moment frames supported on quintuple friction pendulum bearings for nonlinear response history analysis. *J Earthq Tsunami* 2023;17:2350002. <https://doi.org/10.1142/S1793431123500021>.
- [12] ASCE AS. Minimum design loads for buildings and other structures 2010. <https://doi.org/10.1061/9780784412916>.
- [13] Loads MD. Associated Criteria for Buildings and Other Structures, ASCE 7-16: American Society of Civil Engineers. Struct Eng Institute, Reston, Virginia, USA 2017. <https://doi.org/10.1061/9780784414248>.
- [14] Sayani PJ, Erduran E, Ryan KL. Comparative response assessment of minimally compliant low-rise base-isolated and conventional steel moment-resisting frame buildings. *J Struct Eng* 2011;137:1118–31. [https://doi.org/10.1061/\(ASCE\)ST.1943-541X.0000358](https://doi.org/10.1061/(ASCE)ST.1943-541X.0000358).
- [15] Habib A, Yildirim U. Distribution of strong input energy in base-isolated structures with complex nonlinearity: a parametric assessment. *Multidiscip Model Mater Struct* 2023;19:324–40. <https://doi.org/10.1108/MMMS-08-2022-0158>.
- [16] Habib A, Yildirim U. Influence of isolator properties and earthquake characteristics on the seismic behavior of RC structure equipped with quintuple friction pendulum bearings. *Int J Struct Stab Dyn* 2023;23:2350060. <https://doi.org/10.1142/S0219455423500608>.
- [17] Naaseh S, Morgan TA, Walters MT. A critical evaluation of current US building code provisions and FEMA guidelines for the design of seismic isolated structures. *Proc. ATC 17-2 Semin. Seism. Isol. Passiv. Energy Dissipation Act. Control*, 2002.
- [18] Habib A, Yildirim U. Proposing unsupervised clustering-based earthquake records selection framework for computationally efficient nonlinear response history analysis of structures equipped with multi-stage friction pendulum bearings. *Soil Dyn Earthq Eng* 2024;182:108732. <https://doi.org/10.1016/j.soildyn.2024.108732>.
- [19] Vibhute AS, Bharati SD, Shrimali MK, Datta TK. Optimum coefficient of friction in FPS for base isolation of building frames. *Pract Period Struct Des Constr* 2022;27:4022042. [https://doi.org/10.1061/\(ASCE\)SC.1943-5576.0000722](https://doi.org/10.1061/(ASCE)SC.1943-5576.0000722).
- [20] Di Sarno L, Chioccarelli E, Cosenza E. Seismic response analysis of an irregular base isolated building. *Bull Earthq Eng* 2011;9:1673–702. <https://doi.org/10.1007/s10518-011-9267-1>.
- [21] Mazza F, Donnici A, Labernarda R. Seismic vulnerability of fixed-base and base-isolated hospitals: blind comparison between shaking table and numerical tests. *Procedia Struct Integr* 2023;44:147–54. <https://doi.org/10.1016/j.prostr.2023.01.020>.
- [22] Ghorbi E, Toopchi-Nezhad H. Annular fiber-reinforced elastomeric bearings for seismic isolation of lightweight structures. *Soil Dyn Earthq Eng* 2023;166:107764. <https://doi.org/10.1016/j.soildyn.2023.107764>.

- [23] Losanno D, Ravichandran N, Parisi F. Seismic fragility of base-isolated single-storey unreinforced masonry buildings equipped with classical and recycled rubber bearings in Himalayan regions. *J Build Eng* 2022;45:103648. <https://doi.org/10.1016/j.jobe.2021.103648>.
- [24] Belbachir A, Benanane A, Ouazir A, Harrat ZR, Hadzima-Nyarko M, Radu D, et al. Enhancing the seismic response of residential RC buildings with an innovative base isolation technique. *Sustainability* 2023;15:11624. <https://doi.org/10.3390/su151511624>.
- [25] Ding X, Liapopoulou M, Elghazouli AY. Seismic response of non-structural components in multi-storey steel frames. *J Constr Steel Res* 2024;213:108398. <https://doi.org/10.1016/j.jcsr.2023.108398>.
- [26] Chimamphant S, Kasai K. Comparative response and performance of base-isolated and fixed-base structures. *Earthq Eng & Struct Dyn* 2016;45:5–27. <https://doi.org/10.1002/eqe.2612>.
- [27] Nie G, Wang W, Zhang C, Zhi X, Liu K. Seismic evaluation of isolation performance on single layer cylindrical reticulated shells supported along four sides. *Eng Struct* 2024;301:117279. <https://doi.org/10.1016/j.engstruct.2023.117279>.
- [28] Sreeman D, Kumar Roy B. Optimization study of isolated building using shape memory alloy with friction pendulum system under near-fault excitations. *Int J Eng* 2022;35:2176–85. <https://doi.org/10.5829/ije.2022.35.11b.12>.
- [29] Kitayama S, Constantinou MC. Collapse performance of seismically isolated buildings designed by the procedures of ASCE/SEI 7. *Eng Struct* 2018;164:243–58. <https://doi.org/10.1016/j.engstruct.2018.03.008>.
- [30] Zhang Y, Guo Z, Liu D, Sun W. Seismic response analysis of super-high-rise building structures with three-layer isolation systems. *Sci Rep* 2023;13:19165. <https://doi.org/10.1038/s41598-023-46207-8>.
- [31] Fenz DM. Development, implementation and verification of dynamic analysis models for multi-spherical sliding bearings. Technical report No. Multidisciplinary Center for Earthquake Engineering Research (MCEER), University at Buffalo, New York, America, Rep. 08-0018; 2008.
- [32] Mazzoni S. OpenSees command language manual. Pacific Earthq Eng Res Cent 2006.
- [33] Fagà E, Ceresa P, Nascimbene R, Moratti M, Pavese A. Modelling curved surface sliding bearings with bilinear constitutive law: effects on the response of seismically isolated buildings. *Mater Struct* 2016;49:2179–96. <https://doi.org/10.1617/s11527-015-0642-2>.
- [34] ASCE. NEES-TIPS 2008. [https://ascelibrary.org/doi/abs/10.1061/41000\(315\)14](https://ascelibrary.org/doi/abs/10.1061/41000(315)14).
- [35] Shakouri A, Amiri GG, Salehi M. Effects of ductility and connection design on seismic responses of base-isolated steel moment-resisting frames. *Soil Dyn Earthq Eng* 2021;143:106647. <https://doi.org/10.1016/j.soildyn.2021.106647>.
- [36] Jalali Y, Amiri GG, Shakouri A. Comparative response assessment of base-isolated braced-frame buildings considering effects of ductility design. *J Build Eng* 2021;43:103110. <https://doi.org/10.1016/j.jobe.2021.103110>.
- [37] USGS. The USGS Earthquake Hazards Program of the U.S. Geological Survey 2016. <https://earthquake.usgs.gov/ws/designmaps/asce7-16.html>.
- [38] FEMA. NEHRP Recommended Seismic Provisions: Design Examples (FEMA P-1051). Federal Emergency Management Agency: National Earthquake Hazards Reduction Program, VA, U.S.A; 2017.
- [39] Constantinou MC, Kalpakidis I V, Filiatrault A, Lay RAE. LRFD-based analysis and design procedures for bridge bearings and seismic isolators. Technical Report Multidisciplinary Center for Earthquake Engineering Research (MCEER), Buffalo, New York, America, Rep. 11-0004; 2011.
- [40] Habib A, Hourri AAL, Habib M, Elzokra A, Yildirim U. Structural performance and Finite Element modeling of roller compacted concrete dams: A review. *Lat Am J Solids Struct* 2021;18:e376. <https://doi.org/10.1590/1679-78256467>.
- [41] Habib M, Bashir B, Als Salman A, Bachir H. Evaluating the accuracy and effectiveness of machine learning methods for rapidly determining the safety factor of road embankments. *Multidiscip Model Mater Struct* 2023;19:966–83. <https://doi.org/10.1108/MMMS-12-2022-0290>.
- [42] Habib A, Barakat S, Al-Toubat S, Junaid MT, Maalej M. Developing machine learning models for identifying the failure potential of fire-exposed FRP-strengthened concrete beams. *Arab J Sci Eng* 2024;1–16. <https://doi.org/10.1007/s13369-024-09497-2>.

- [43] McKenna F. OpenSees: a framework for earthquake engineering simulation. *Comput Sci & Eng* 2011;13:58–66. <https://doi.org/10.1109/MCSE.2011.66>.
- [44] Hosseini SM, Hadi K. Application of Opensees Software in Structural Modeling and Analysis 2013.
- [45] Chang GA, Mander JB. Seismic energy based fatigue damage analysis of bridge columns: Part 1— Evaluation of seismic capacity. National Center for Earthquake Engineering Research Technical Report, University of Central Florida Department of Civil and Environmental Engineering Orlando, Florida, America, Rep. 94-0006; 1994.
- [46] Dodd LL, Restrepo-Posada JI. Model for predicting cyclic behavior of reinforcing steel. *J Struct Eng* 1995;121:433–45. [https://doi.org/10.1061/\(ASCE\)0733-9445\(1995\)121:3\(433\)](https://doi.org/10.1061/(ASCE)0733-9445(1995)121:3(433)).
- [47] Hosseini-Gelekolai SM, Tabeshpour M. Soft story design in reinforced concrete structure and effect of masonry infill wall. Proceedings, sixth Int. Conf. Seismol. Earthq. Eng. CDROM Tehran, Iran, 2011, p. 1–18.
- [48] Hosseini Gelekolai SM, Golafshani AA, Tabeshpour MR. Design of Soft Story in Reinforced Concrete Structure due to Removal of Masonry Infill Wall. Sharif Univ Technol 2010.
- [49] Liu M, Gorman DG. Formulation of Rayleigh damping and its extensions. *Comput & Struct* 1995;57:277–85. [https://doi.org/10.1016/0045-7949\(94\)00611-6](https://doi.org/10.1016/0045-7949(94)00611-6).
- [50] Ryan KL, Polanco J. Problems with Rayleigh damping in base-isolated buildings. *J Struct Eng* 2008;134:1780–4. [https://doi.org/10.1061/\(ASCE\)07339445\(2008\)134:11\(1780\)](https://doi.org/10.1061/(ASCE)07339445(2008)134:11(1780)).
- [51] Constantinou MC, Tsopelas P, Kasalanati A, Wolff ED. Property modification factors for seismic isolation bearings. Multidisciplinary Center for Earthquake Engineering Research, State University of New York, Rep. 99-0012; 1999.
- [52] PEER. Pacific Earthquake Engineering Research Center Strong Motion Database on Line. Berkley 2016. <https://peer.berkeley.edu/peer-strong-ground-motion-databases>.